

Phase Imprinting in Equilibrating Fermi Gases: The Transience of Vortex Rings and Other Defects

Peter Scherpelz,¹ Karmela Padavić,¹ Adam Rançon,¹ Andreas Glatz,² Igor S. Aranson,² and K. Levin¹

¹*James Franck Institute and Department of Physics,
University of Chicago, Chicago, Illinois 60637, USA*

²*Materials Science Division, Argonne National Laboratory,
9700 South Cass Avenue, Argonne, Illinois 60439, USA*

(Dated: December 3, 2024)

We present numerical simulations of phase imprinting experiments in ultracold trapped Fermi gases. The dynamics we consider is associated with a time-dependent Ginzburg-Landau equation, which contains dissipation (arising from fermionic dissociation of the pairs) as well as a noise contribution. In contrast to other simulations we find that vortex rings in confined geometries are highly transient. Small noise-induced asymmetries in their position within the trap lead to their migration to the trap surface and subsequent decay into vortex lines. In the simplest terms this follows because asymmetrically positioned rings are attracted to “quasi-image” rings which leads to their reconnection, leaving more stable, precessing vortex filaments behind.

Introduction. There has been a focus in recent literature on collective defects in trapped, cold gas superfluids following sudden changes in density or in superfluid phase. Bosonic studies have reported solitons [1–3] which generally decay rapidly. Recently these same experimental techniques have been applied to Fermi gases in the BCS-to-BEC crossover. Surprisingly there are reports of rather long-lived solitons with anomalously large effective masses [4] reflecting long oscillation periods. Theoretical work based on numerical simulations of the Gross-Pitaevskii (GP) and Bogoliubov-de Gennes (BdG) equations has addressed this unexpected stability and attributed it to vortex rings rather than solitonic defects [5, 6]. This observation, in turn, appears to be at odds with studies of vortex rings in Bose gases where it is claimed that they, like their solitonic counterparts, are short lived [3, 7].

In this paper we present simulations for Fermi gases using a phenomenological time-dependent Ginzburg-Landau theory describing dissipative relaxation processes. Our central finding is that all vortex rings (as well as solitons) are rather transient. We do not observe the very stable ring oscillations reported by other theory groups. Instead, we find that an axially moving ring formed through phase imprinting is unstable, as shown in Figure 1(a-b). This is revealed by considering a small noise contribution which breaks the axial symmetry causing the ring (through image effects, and through advection by the super-currents generated via imprinting) to rise to the trap surface. There it decays into a single and more stable vortex line which then precesses about the cloud. As will be discussed in this paper, we speculate that this line defect and its precessional dynamics may be relevant to recent experimental observations [4].

One can understand the defect formations and subsequent decays that we study here as a series of processes in which the system becomes progressively closer to equilibration. While other simulations have identified the

soliton to vortex ring transition, past simulations (omitting noise and dissipation) do not appear to exhibit all the transitions necessary for the full equilibration of the cloud. The literature [5, 6] has focused on symmetric vortex rings which maintain inversion symmetry about the z -axis [parity transformation (x, y) to $(-x, -y)$] and often apply initial conditions specifically designed to produce a stable vortex ring.

Our approach. Here we study the complex time-dependent Ginzburg-Landau (TDGL) equation [8], $e^{-i\theta}\partial_t\psi(\mathbf{x}, t) =$

$$\left\{ [1 - V(\mathbf{x})] + \frac{1}{2}\nabla^2 - |\psi(\mathbf{x}, t)|^2 \right\} \psi(\mathbf{x}, t) + \chi(\mathbf{x}, t), \quad (1)$$

when three-dimensional (3D) anisotropic trapped Fermi gases are subjected to a near- π phase imprinting quench [4]. Here V is the harmonic potential and χ is uniformly distributed thermal noise. Equation (1) contains four parameters. First, θ controls the amount of dissipation, effectively moving from BCS ($\theta = 0$, dissipative) to BEC ($\theta = \pi/2$, reducing to the time-dependent GP equation). Second, in the harmonic confining potential $V(\mathbf{x}) = (\omega_\perp^2(x^2 + y^2) + \omega_z z^2)/2$, ω_\perp and ω_z define how tightly confining the trap is in comparison to the chemical potential, as well as the trap ratio $\lambda = \omega_\perp/\omega_z$. Finally, through $\langle \chi(\mathbf{x}, t)\chi^*(\mathbf{x}', t') \rangle = 2\gamma T_\chi \delta(\mathbf{x} - \mathbf{x}')\delta(t - t')$, a fluctuation temperature can be set [9–12]. In this work the dimensionless fluctuation temperature is chosen to be very close to the zero-temperature limit, with $\gamma T_\chi = 2 \times 10^{-9}$ [11]. Beyond these parameters, the rescaling to this normalized form follows from Ref. [8].

A TDGL approach [14–16] can be viewed as a dissipative GP simulation where the dissipation becomes progressively stronger as the dynamics changes from propagating (in BEC) to diffusive (in BCS), reflecting the fact that pairs are in equilibrium with the underlying fermions. Along with this dissipation is a stochastic contribution required for full consistency [11]. For the Fermi

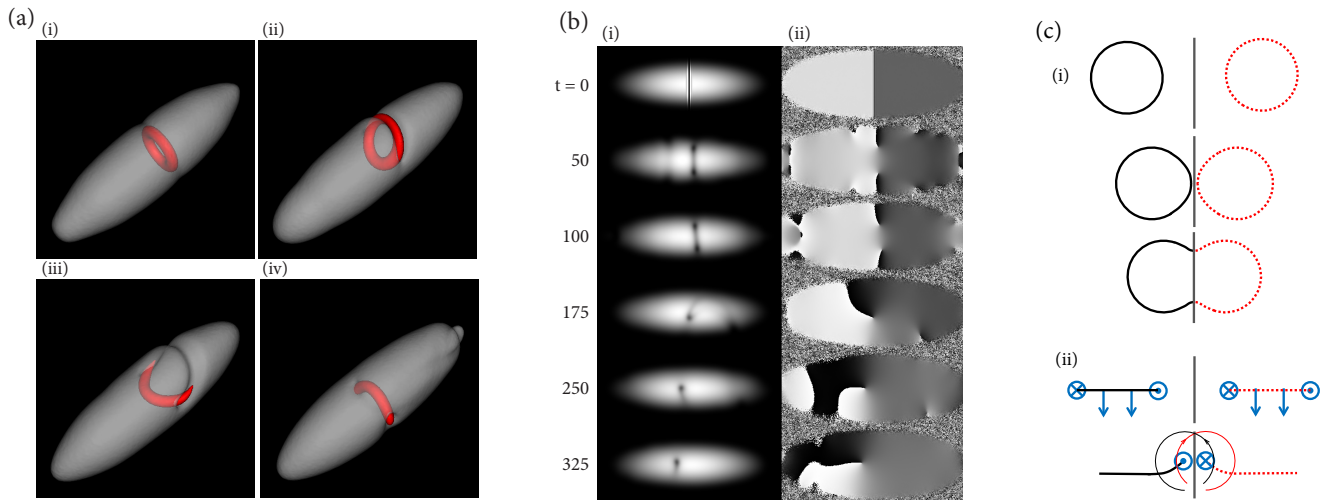


FIG. 1. (Color online) (a-b) TDGL simulation results for one time sequence, focusing on the vortex ring decay, of a phase imprinting applied at $t = 0$ with $\lambda = 3.3$ and parameters as in the text. (a) 3D perspective views of the cloud during vortex ring decay are shown. White is used for a semi-transparent isosurface of $|\psi|^2$, while red highlights density depletions by plotting an isosurface of $|\psi_e|^2 - |\psi|^2$, where $|\psi_e|^2$ is the equilibrium cloud density. Here phase imprinting has formed a ring (a.i), which is just slightly off center. The ring moves toward the cloud edge (a.ii), then impacts the edge and decays to a vortex line (a.iii-iv). (b) Plotted run results, with (b.i) the cloud density integrated along y and (b.ii) the phase in the $y = 0$ plane [from 0 (black) to 2π (white)]. (c) Illustration of a vortex ring (black) to image ring (dotted red) reconnection process [13], from top to bottom and viewed along the z axis in (c.i). Panel (c.ii) shows the side view parallel to the boundary plane and vortex ring plane. Circulation corresponds to $\{\odot, \otimes\}$ for counterclockwise and clockwise rotation, respectively, in this view. Arrows indicate velocities induced by the vortex ring segments nearest the surface.

gases simulated here, earlier estimates of the TDGL coefficients [14] have been modified through higher levels of microscopic self-consistency, leading to longer-lived pairs in the intermediate (near-unitary) regime [15, 16]. This increases θ , and we frequently used $\theta = 88^\circ$ for unitarity, to enhance the stability and visibility of the various defects.

The precise form and rescaling of the trap potential is inserted via the local density approximation, $\mu \rightarrow \mu - V(\mathbf{x})$, where μ is the chemical potential [normalized to 1 in Eq. (1)]. In the bosonic TDGL limit, this trap potential form is identical to that used in GP [17], and away from this limit, it is slightly rescaled.

Our studies are based on numerical simulations discretized in 512^3 grid points designed to solve Equation (1) using a quasi-spectral split-step method. The simulations are performed on a GPU computing cluster, allowing relatively large simulation sizes. The initial condition is found using a heat diffusion equation to cool the system to equilibrium before the phase imprinting is applied, as in Ref. [11].

Ring decay via reconnection with image vortex rings. We demonstrate that the vortex ring decay in Figure 1(a-b) can be viewed schematically as a consequence of the attraction to an image ring vortex (necessary to ensure the boundary conditions are satisfied [13]). Effectively, the ring at the surface reconnects with its image, which leads the ring to decay into a single vortex filament

within the trap. Figure 1(c) illustrates the reconnection of a vortex ring (black) to the image ring (dotted red) for the straightforward case of a sharp, planar boundary. While the ring propagates along the boundary due to advection by supercurrents, the image vortex retards that part nearest the boundary leading to a tilt as it reconnects, as seen in Figure 1(a). This results in a vortex line attached to the boundary. The dynamics are essentially the same as that of the reconnection between two lines [13, 18, 19].

We use the method of images by considering the interactions of a hard boundary which is approximated as a plane. Although this approach is qualitative [20–22] it can provide valuable insight into vortex behavior near boundaries [20] ([23]). Importantly, these image ring arguments match our observations in the above simulations.

To use the method of images with a hard boundary, one begins with the condition that the normal component of the superfluid velocity is zero on the boundary, $\mathbf{v}_s \cdot \mathbf{n} = 0$. The physics is governed by the Biot-Savart law for the velocity fields created by vortices in the absence of boundaries [13]:

$$\mathbf{v}_{s,w}(\mathbf{r}) \equiv \frac{\kappa}{4\pi} \int_{\mathcal{L}} \frac{(\mathbf{s} - \mathbf{r}) \times d\mathbf{s}}{|\mathbf{s} - \mathbf{r}|^3} + \mathbf{v}_{s,i}, \quad (2)$$

where the integral goes over the vortex line(s), κ is the quantized vortex circulation, and $\mathbf{v}_{s,i}$ is due to imprinting. However, to satisfy the boundary condition

$\mathbf{v}_s \cdot \mathbf{n} = 0$, a second (boundary) velocity field $\mathbf{v}_{s,b}$ is added, with $\nabla \cdot \mathbf{v}_{s,b} = 0$ and $\nabla \times \mathbf{v}_{s,b} = 0$, such that

$$(\mathbf{v}_{s,w} + \mathbf{v}_{s,b}) \cdot \mathbf{n} = 0. \quad (3)$$

For a plane boundary, $\mathbf{v}_{s,b}$ is the field created by an image vortex, which is the real vortex reflected along the boundary with the vortex direction reversed [13].

Our detailed findings: Transience of defects. We turn now to a summary of our simulations. We investigated a system with axial (xy) symmetry, $\omega_z = 0.038\mu/\hbar$, and a variable trap ratio $\lambda = \omega_\perp/\omega_z$. The parameters used here match the trap ratios and symmetries in Ref. [4], but with a somewhat larger ω/μ which provides more fine-grained computational resolution of the defects.

We will focus on the case $\lambda = 3.3$. In more anisotropic traps with $\lambda = 6.2$, we find the vortex ring is even more transient, immediately colliding with the cloud edge to leave a line vortex. Finally, in quasi-1D clouds with $\lambda = 15.0$, the system cannot nucleate vortices and a reasonably stable soliton appears which oscillates along the axial direction of the trap, in agreement with 1D predictions.

After the cloud has reached equilibrium, we imprint a 175° phase shift in the middle of the cloud (in a plane perpendicular to z), and observe the evolution. Images from a typical run are displayed in Figure 1(b).

The initial formation of the vortex ring through the snake instability [6, 24–28] appears in the second and third frames of Figure 1(b) [29]. In the absence of noise and dissipation, this ring is stable and oscillates in the trap, as observed in other simulations. The fourth frame reflects the ring collision with the boundary. The presence of noise perturbs part of the ring moving it closer to the boundary. Boundary effects will then tilt the ring due to inhomogeneities of the supercurrent, which is weakest in the center of the condensate, as seen in Figure 1(a.iii) [22, 30]. Boundary effects will also attract the ring to the boundary [which occurs through both boundary-induced (“image”-induced) attraction and through dissipation [30]].

As a final step the reconnection with the quasi-image ring leads to a line vortex attached to the boundary, with additional remnant density perturbations. We note that the decay of a vortex ring to possibly two vortex lines has also been observed recently in the context of non-axisymmetric clouds with larger asymmetries in trap frequencies, ω_x and ω_y [31]. This contrasts with the decay we observe in axisymmetric clouds, for which the ring appears to reconnect with the boundary at just one location and create only a single vortex line.

In Figure 2 we plot the lifetime of these defects as a function of the initial phase imprinting angle applied. The vortex ring always decays relatively rapidly, through shrinking to zero radius at small imprinting angles or from impacting the trap edge at larger angles. Moreover,

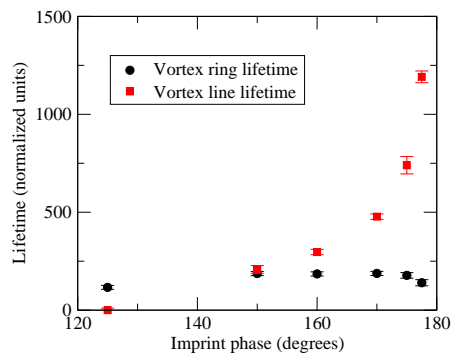


FIG. 2. (Color online) Lifetimes of defects as a function of the imprinting phase, using the same parameters as in Figure 1. Red squares indicate lifetimes of vortex lines, which are substantially longer than those of vortex rings (black circles). Error bars reflect run-to-run variations and limitations on time estimates.

at large phase imprinting angles, the vortex line that remains after ring decay can persist for a relatively long time, as in Figure 3(a). Indeed, we find that this more stable vortex filament may precess about the cloud three or more times before it collides with the edge, where it decays. These lifetimes also reflect the advection of the defects, which depends on both the local phase gradient and the superfluid density depletion. We find that, similar to solitonic behavior [32], small phase shifts lead to large defect velocities, while phase shifts close to π cause large density depletions and apply very little momentum to the defects. The low defect velocity contributes to the long vortex line lifetime in this regime.

A more detailed view of this precessing trajectory is shown in Figure 3(b). At the earliest times, when the vortex is near the center, it has a smaller-scale rotation in the counterclockwise direction in addition to the main precession of the vortex in the clockwise direction. This smaller-scale rotation, seemingly due to the decay of the other portion of the ring, gradually subsides, and the remaining precession and outward movement of the vortex are typical in the presence of dissipation [30, 33].

We are led to speculate that what might have been observed experimentally [4] is this precessing vortex filament. During the precession, we are able to observe a traveling density depletion, shown in Figure 3(a). We find that the vortex line can appear as a line-like density depletion very similar to experimental images [4]. This apparently oscillating line of density depletion reflects the fact that the vortex line is precessing in a plane that is nearly orthogonal to the one observed. At more oblique, rather than orthogonal, points of view a vortex may still look line-like after a time-of-flight expansion of the anisotropic trap [4, 5].

We have shown how phase imprinting, such as that studied in Ref. [4], created a long-lived linear defect.

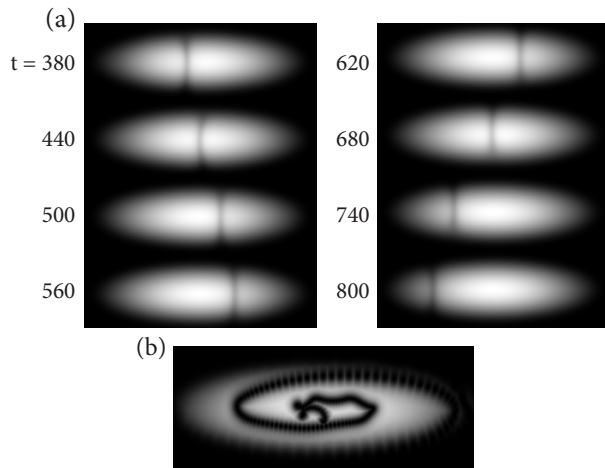


FIG. 3. (a) A series of density plots for the $\lambda = 3.3$ run in Figure 1(a-b), integrated along the x axis, during the interval in which only one vortex is present. The density effectively shows a line depletion due to the orientation of the vortex, which oscillates along the cloud. (b) Plots of the trajectory of the precessing single vortex near the end-stage of equilibration for the same run. Here frames (cuts of $|\psi|^2$ along the $y = 0$ plane) with $\Delta t = 5$ were combined and the minimum density among all frames selected, displaying the vortex trajectory during $t = [180, 1160]$.

However, the relevance of this vortex line to experiment should be reflected in the period of oscillations and the associated trends from the BCS to BEC sides of unitarity. In general, we expect that for constant trap parameters, the period of the precession of a vortex line will follow the size of the superfluid cloud. This means that as the system approaches unitarity from the BEC side, the increase in interaction strength will expand the cloud and lead to a longer precession period. Similarly, if ω_{\perp} is kept constant and λ decreased, the weaker z -axis confinement will increase the cloud size and lead to a longer precession period. Both of these trends match the BCS-BEC variation observed experimentally [4].

These predictions can be quantified using the Thomas-Fermi (TF) approximation. In this case the precession frequency has been derived as [34–36]

$$\omega_p = \frac{3\hbar\omega_z\omega_{\perp}}{M(\omega_z^2 + \omega_{\perp}^2)R_{xz}^2} \log\left(\frac{R_{xz}}{\xi}\right) \frac{1}{1 - r_0^2}, \quad (4)$$

where ξ is the healing length, $R_{xz}^2 = 4\mu/[M(\omega_z^2 + \omega_{\perp}^2)]$ defines an effective trap radius, and $r_0 = (x/R_x, z/R_z)$ is the dimensionless vortex position. Using the TF approximation [17] for the parameters μ and ω_{\perp} given in Ref. [4] at unitarity, we obtain a very rough estimate of the ratio of the vortex period to the trap period as $T_v/T_z = 10.2/(1 - r_0^2)$, in reasonable agreement with the reported results near unitarity.

For our simulations (with smaller μ/ω_{\perp} values), the above approximation predicts $T_v/T_z = \{3.5, 2.3\}(1 - r_0^2)$

for $\lambda = \{3.3, 6.2\}$ respectively. We measured an average $T_v/T_z = \{2.4 \pm 0.3, 1.6 \pm 0.2\}$ for these λ , which agree for $r_0 \approx 0.7$. We also observed the predicted decrease in period as the vortex moves to larger radii. Furthermore, although the vortex ring exhibited the slowest oscillation of the defects considered (we reduced noise to 0 and observed $T_{vr}/T_z = 1.8 \pm 0.2$ for $\lambda = 6.2$), the distinction between it and the line vortex is not large, and we do not consider the oscillatory period found in the experiment to point to definitive proof of a vortex ring [37]. Finally, for the quasi-1D case with $\lambda = 15$, we find $T_s/T_z = 1.39 \pm 0.03$, in good agreement with the predicted $T_s/T_z = \sqrt{2}$ value for the GP system.

Conclusion. It remains to be seen as to whether the more stable vortex lines which we find are relevant to experiment [4]. In general we find that the vortex line is most likely to lie parallel to the most confining trap direction. Thus, asymmetries between the trap frequencies, ω_x and ω_y , if they are sufficiently large [31], may further bias experimental observations toward visualization of a line. Added to these considerations is the fact that the oscillation period associated with the precessing vortex filament [Eq. (4)] depends directly on the cloud size squared, and that this period will be longest in the BCS and shortest in the BEC regimes. In these respects, therefore, the behavior observed in our simulations reflects that found experimentally [4], although here we attribute it to a linear rather than planar defect.

We stress that independent of past or future experimental findings, we have shown in this work how noise and related dissipation mechanisms can have a profound effect on defects in cold gases. In addressing phase imprinting experiments it is essential that a theory include this dissipation to account for an ultimate equilibration.

This work is supported by NSF-MRSEC Grant 0820054. Work at Argonne was supported by the Scientific Discovery through Advanced Computing (SciDAC) program funded by U.S. Department of Energy, Office of Science, Advanced Scientific Computing Research and Basic Energy Sciences, and by the Office of Science, Materials Sciences and Engineering Division. The numerical work was performed on NIU's GPU cluster GAEA. P.S. acknowledges support from the Hertz Foundation. Finally, we are grateful to William Irvine and Ariel Sommer for insightful discussions.

-
- [1] S. Burger, K. Bongs, S. Dettmer, W. Ertmer, K. Sengstock, A. Sanpera, G. V. Shlyapnikov, and M. Lewenstein, Phys. Rev. Lett. **83**, 5198 (1999).
 - [2] J. Denschlag, J. E. Simsarian, D. L. Feder, C. W. Clark, L. A. Collins, J. Cubizolles, L. Deng, E. W. Hagley,

- K. Helmerson, W. P. Reinhardt, S. L. Rolston, B. I. Schneider, and W. D. Phillips, *Science* **287**, 97 (2000).
- [3] B. P. Anderson, P. C. Haljan, C. A. Regal, D. L. Feder, L. A. Collins, C. W. Clark, and E. A. Cornell, *Phys. Rev. Lett.* **86**, 2926 (2001).
- [4] T. Yefsah, A. T. Sommer, M. J. H. Ku, L. W. Cheuk, W. Ji, W. S. Bakr, and M. W. Zwierlein, *Nature* **499**, 426 (2013).
- [5] A. Bulgac, M. M. Forbes, M. M. Kelley, K. J. Roche, and G. Wlazlowski, *Phys. Rev. Lett.* **112**, 025301 (2014).
- [6] M. D. Reichl and E. J. Mueller, arXiv:1309.7012.
- [7] A. I. Yakimenko, Y. M. Bidasyuk, O. O. Prikhodko, S. I. Vilchinskii, E. A. Ostrovskaya, and Y. S. Kivshar, *Phys. Rev. A* **88**, 043637 (2013).
- [8] I. S. Aranson and L. Kramer, *Rev. Mod. Phys.* **74**, 99 (2002).
- [9] I. S. Aranson, N. B. Kopnin, and V. M. Vinokur, *Phys. Rev. Lett.* **83**, 2600 (1999).
- [10] B. Damski and W. H. Zurek, *Phys. Rev. Lett.* **104**, 160404 (2010).
- [11] A. Glatz, H. L. L. Roberts, I. S. Aranson, and K. Levin, *Phys. Rev. B* **84**, 180501 (2011).
- [12] A. Schmid, *Phys. Rev.* **180**, 527 (1969).
- [13] K. W. Schwarz, *Phys. Rev. B* **31**, 5782 (1985).
- [14] C. A. R. Sá de Melo, M. Randeria, and J. R. Engelbrecht, *Phys. Rev. Lett.* **71**, 3202 (1993).
- [15] J. Maly, B. Jankó, and K. Levin, *Physica C: Superconductivity* **321**, 113 (1999).
- [16] J. Maly, *Pseudogap effects in a precursor superconductivity model of the cuprates*, Ph.D. thesis, The University of Chicago, United States – Illinois (1997).
- [17] C. Pethick and H. Smith, *Bose-Einstein Condensation in Dilute Gases*, 2nd ed. (Cambridge University Press, Cambridge, 2008).
- [18] E. D. Siggia, *Phys. Fluids* **28**, 794 (1985).
- [19] J. Koplik and H. Levine, *Phys. Rev. Lett.* **71**, 1375 (1993).
- [20] P. Mason and N. G. Berloff, *Phys. Rev. A* **77**, 032107 (2008).
- [21] P. Mason, N. G. Berloff, and A. L. Fetter, *Phys. Rev. A* **74**, 043611 (2006).
- [22] J. R. Anglin, *Phys. Rev. A* **65**, 063611 (2002).
- [23] While Ref. [22] argues against the use of image vortices for quantitative work in trapped gases, the author does acknowledge their qualitative predictions are usually accurate. Furthermore, Ref. [20] is able to use image vortices to analyze essentially the same problem.
- [24] C. A. Jones, S. J. Putterman, and P. H. Roberts, *J. Phys. A* **19**, 2991 (1986).
- [25] A. V. Mamaev, M. Saffman, and A. A. Zozulya, *Phys. Rev. Lett.* **76**, 2262 (1996).
- [26] A. V. Mamaev, M. Saffman, D. Z. Anderson, and A. A. Zozulya, *Phys. Rev. A* **54**, 870 (1996).
- [27] V. Tikhonenko, J. Christou, B. Luther-Davies, and Y. S. Kivshar, *Opt. Lett.* **21**, 1129 (1996).
- [28] D. L. Feder, M. S. Pindzola, L. A. Collins, B. I. Schneider, and C. W. Clark, *Phys. Rev. A* **62**, 053606 (2000).
- [29] Sound waves are also produced by phase imprinting, but dissipate as they reach the trap edge. This agrees with experimental observations [4] and is in contrast to the behavior of sound modes in GP simulations [5, 6].
- [30] N. G. Parker, B. Jackson, A. M. Martin, and C. S. Adams, in *Emergent Nonlinear Phenomena in Bose-Einstein Condensates*, Atomic, Optical, and Plasma Physics No. 45, edited by P. P. G. Kevrekidis, P. D. J. Frantzeskakis, and P. R. Carretero-González (Springer Berlin Heidelberg, 2008) pp. 173–189.
- [31] C. Becker, K. Sengstock, P. Schmelcher, P. G. Kevrekidis, and R. Carretero-Gonzalez, arXiv:1308.2994.
- [32] T. Busch and J. R. Anglin, *Phys. Rev. Lett.* **84**, 2298 (2000).
- [33] B. Jackson, J. F. McCann, and C. S. Adams, *Phys. Rev. A* **61**, 013604 (1999).
- [34] A. L. Fetter and J.-k. Kim, *J. Low Temp. Phys.* **125**, 239 (2001).
- [35] A. A. Svidzinsky and A. L. Fetter, *Phys. Rev. Lett.* **84**, 5919 (2000).
- [36] A. L. Fetter and A. A. Svidzinsky, *J. Phys. Condens. Matter* **13**, R135 (2001).
- [37] Note that for this run, double precision was used but with a smaller computational grid of edge size $L = 256$ rather than $L = 512$ used in the rest of the paper.

Supplementary Material

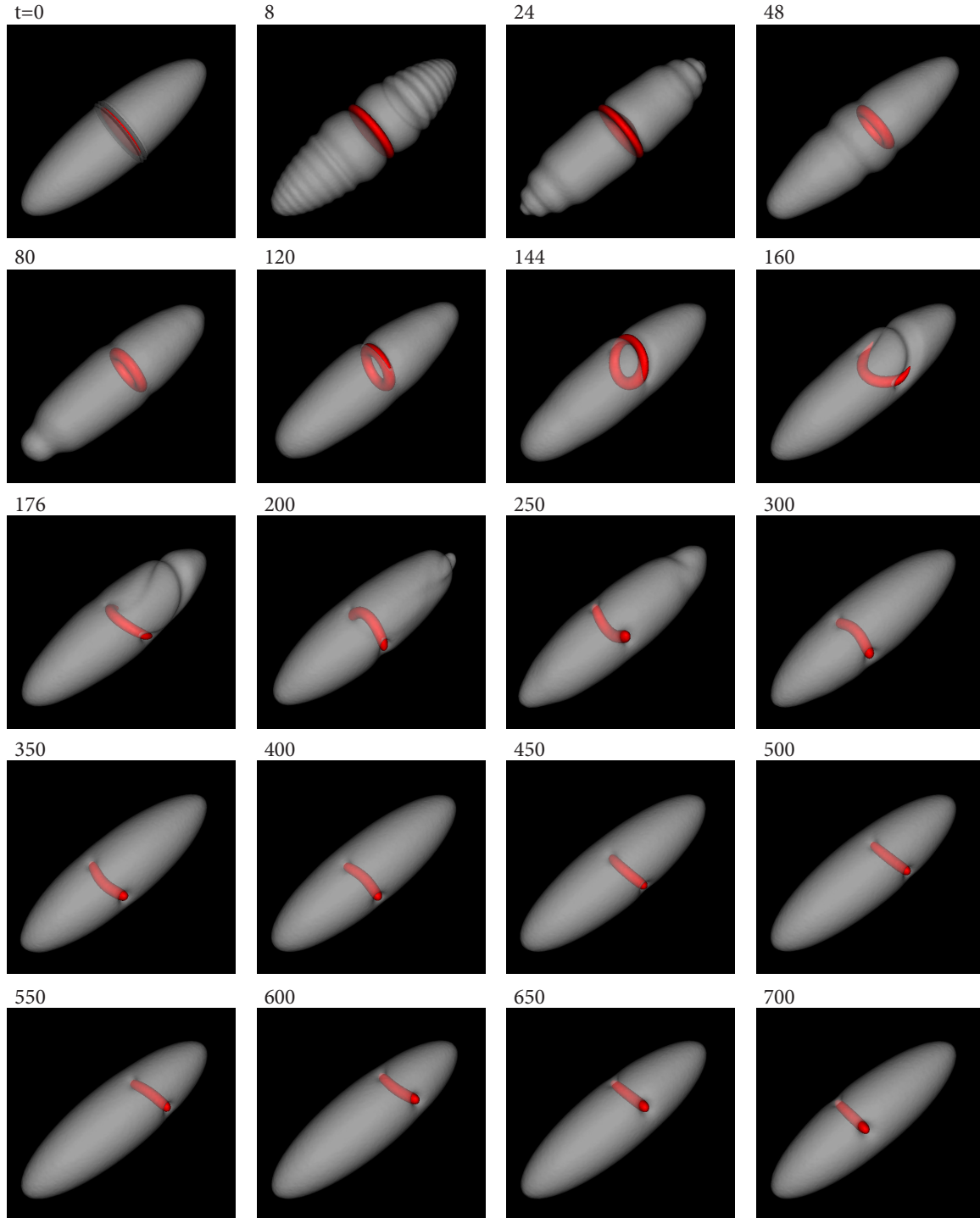


FIG. 1. A time sequence of 3D images for the run in Figure 1(a-b) at the indicated times. Each timestep includes an isosurface of $|\psi|^2$ (white) and of $|\psi_e|^2 - |\psi|^2$ (red), as in Figure 1(a).